

Schwoebel barriers on Si(111) steps and kinks

S. Kodiyalam, K.E. Khor and S. Das Sarma

Department of Physics, University of Maryland, College Park, Maryland 20742-4111

Motivated by our previous work using the Stillinger-Weber potential, which shows that the $\bar{2}11$ step on 1×1 reconstructed Si(111) has a Schwoebel barrier of 0.61 ± 0.07 eV, we calculate here the same barrier corresponding to two types of kinks on this step - one with rebonding between upper and lower terrace atoms (type B) and the other without (type A). From the binding energy of an adatom, without additional relaxation of other atoms, we find that the Schwoebel barrier must be less than 0.39 eV (0.62 eV) for the kink of type A (type B). From the true adatom binding energy we determine the Schwoebel barrier to be 0.15 ± 0.07 eV (0.50 ± 0.07 eV). The reduction of the Schwoebel barrier due to the presence of rebonding along the step edge or kink site is argued to be a robust feature. However, as the true binding energy plots show discontinuities due to significant movement of atoms at the kink site, we speculate on the possibility of multi-atom processes having smaller Schwoebel barriers.

I. INTRODUCTION

The Schwoebel barrier, which was introduced as the additional barrier for adatom diffusion over a step edge from the upper to lower terraces,¹ has been a subject of current interest for its influence on the growth of a singular (flat) surface.²⁻⁶ It was pointed out by Villain⁷ that in the presence of such a barrier, growth of by step flows was stable only if the surface was sufficiently vicinal with possible instabilities setting in during the growth of a flat surface. It is now accepted that it leads to a coarsening of the evolving surface morphology.²⁻⁶ The present study is motivated by recent observations of another kind of instability on the high temperature 1×1 phase of Si(111) - the reversible step bunching instability during sublimation.^{8,9} As these experiments can be reinterpreted in the presence of the Schwoebel barrier,¹⁰ we summarize here our previous calculations of the same corresponding to straight (high symmetry) steps¹⁰ and present results corresponding to kinked steps, both of which use the empirical Stillinger-Weber potential. The use of this potential here (and in our previous¹⁰) study has been motivated by the fact that features that follow from changes in coordination number (of the adatom probing the potential energy topography) are expected to survive even if the details of the empirical potential used change. We attempt to identify such features here.

Table 1 summarizes our previous results.¹⁰ The straight (high symmetry) $\bar{2}11$ and $\bar{1}12$ and other step orientations are shown in Fig.1. Note that the $\bar{2}11$ step

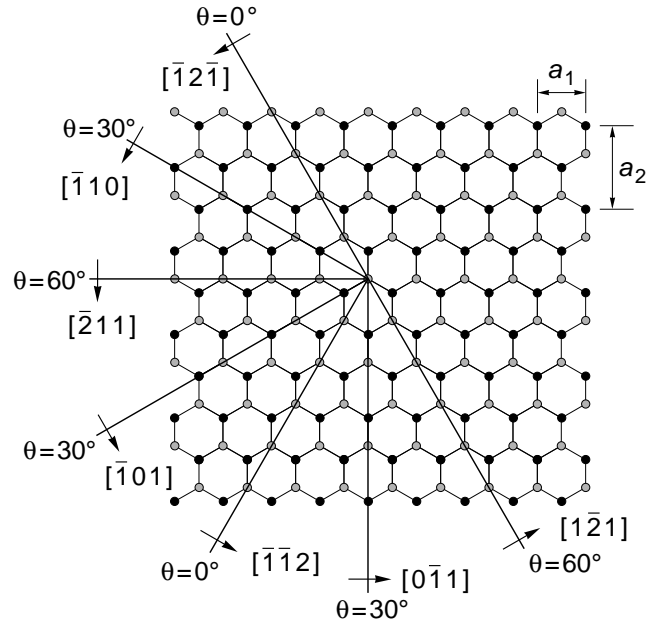


FIG. 1. One bilayer of the Si(111) surface consisting of the upper monolayer (grey) and lower monolayer (black). The figure shows the threefold and reflection symmetry of this surface: Steps running along directions with equal θ are identical.

TABLE 1. V is the adatom potential energy. Shown here is its value at the relevant minimum and saddle points.

Global minimum in $V = -3.31\pm 0.05$ eV			
Configuration	V at saddle point (eV)	\Rightarrow Diffusion barrier (eV)	\Rightarrow Schwoebel barrier (eV)
Si(111) surface	-2.34 ± 0.05	0.97 ± 0.07	-
$\bar{2}11$ step	-1.73 ± 0.05	1.58 ± 0.07	0.61 ± 0.07
$\bar{1}12$ step	-2.18 ± 0.05	1.13 ± 0.07	0.16 ± 0.07

shows a large Schwoebel barrier of 0.61 ± 0.07 eV. However, an analysis of experimental data on the electromigration of steps⁹ using a diffusion equation showed that the upper bound on the Schwoebel barrier¹⁰ (in a particular limit of the equation parameters) was very small (0.05 eV). Therefore, here we calculate the Schwoebel barrier corresponding to unit depth kinks on the $[\bar{2}11]$ step to determine if it continues to be large.

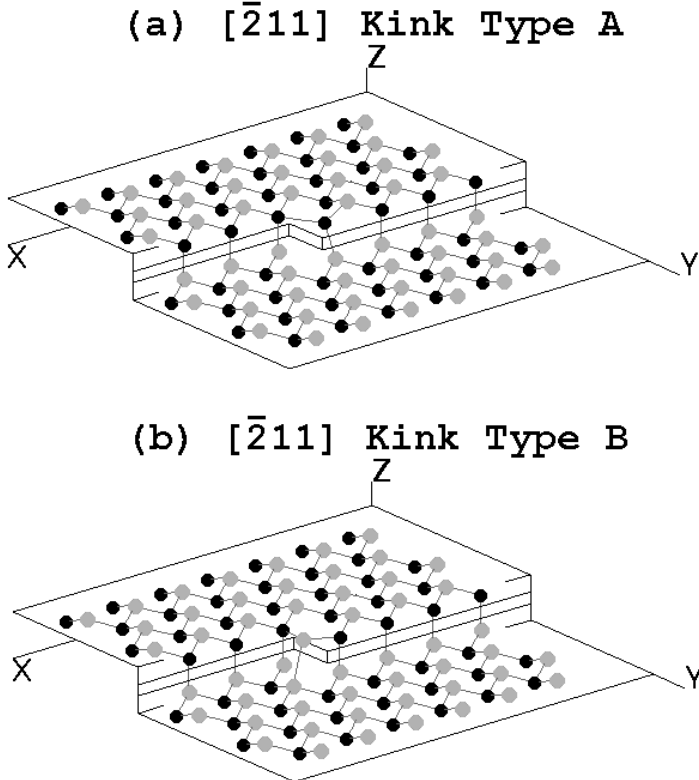


FIG. 2. The two kinks studied here - type A has atoms rebonded along the kink site whereas type B has, at the kink site, an upper terrace atom rebonded to the lower terrace. On both terraces the upper monolayer is shown in grey and the lower monolayer in black.

II. MOLECULAR DYNAMICS METHOD

Using the Stillinger-Weber potential, diffusion barriers are determined by mapping the adatom potential energy a function of the (x, y) position of the adatom (in the (111) plane) for two types of kinks on the $[\bar{2}11]$ step - type A (see Fig. 2(a)), which has rebonding of atoms along the kink site and type B (see Fig. 2(b)), which has, at the kink site, an upper terrace atom rebonded to the lower terrace. In our previous study on straight steps¹⁰, configurations of type B were neglected since the step ($[\bar{1}\bar{1}2]$) that allowed for this structure would have very large step-step interactions inconsistent with experimental estimates.¹¹ However, the large interactions were due to the presence of one rebonding atom per lattice constant along the step edge. The configuration of type B

is nevertheless considered here, since, at low kink densities *i.e.* for a nearly straight $[\bar{2}11]$ step, the number of such rebonding atoms per unit length along the step edge would be correspondingly low and therefore the expected step-step interactions would be smaller. The adatom potential energy V has been computed as the difference in the minimum potential energy of the system with the adatom at infinity (non-interacting) and the same with the interacting adatom.

Standard molecular dynamics (MD) procedures of integrating Newton's law (with dissipation to reduce temperature) and the steepest descent equations have been used to determine the minimum potential energy of the system. These routines determined the adatom potential energy to an accuracy of 10^{-4} eV. The (x, y) coordinates of the adatom are fixed during the integration process. The system consisted (as before¹⁰) of six bilayers of Si(111) in an MD cell, the bottom three layers of which are fixed at bulk lattice coordinates throughout the calculation. The system size along the x axis (ℓ_x) (which was parallel the $[\bar{2}11]$ step edge) was $5\frac{1}{2}a_1$ and along the y axis (ℓ_y) was $3\frac{2}{3}a_2$. Periodic boundary conditions along the x axis identified the points $(0, 0, h)$ (h is the step height) and $(0, \ell_y, 0)$ and the same along the y axis identified the points $(0, k, 0)$ (k is the kink depth) and $(\ell_x, 0, 0)$. These boundary conditions made it possible to have exactly one vicinal step with one kink (and no antikinks) in the MD cell. As before,¹⁰ the atoms on the (x, y) boundaries were however held fixed during the computation of V to prevent the entire configuration from shearing, particularly when the adatom is moved away from a deep minimum. The kinks were roughly in the middle of the cell consisting of movable atoms (see Figs. 3(a) and 4(a)). As the $(x - y)$ size of this cell is larger than that used previously¹⁰ in studying the system size dependence of V on the Si(111) surface and since it is more square in shape, we expect the error in V due to finite size effects to be smaller than before¹⁰ (0.01 eV). It must be additionally noted that with the system size used here (with the adatom absent), the kink energy was within 6 meV (4 meV) of that calculated previously¹¹ for the kink of type A (type B).

The MD procedures began with the initial configurations for each (x, y) position of the adatom corresponding to the relaxed adatom-free structures. The z coordinate of the adatom was then varied in small steps in a wide range to roughly determine the point (z_0) at which its potential energy is the smallest. Initializing this z coordinate at z_0 , the integration procedures were followed, first with only the adatom relaxing while other atoms remain fixed. The minimum of the potential energy reached this way (V_{lg}) depends only on the local geometry of atoms around the adatom. The atoms that were held fixed are then allowed to relax together with the adatom to recompute the minimum which is now the true adatom potential energy (V). With the kink roughly in the middle of the region explored (see Figs. 3(b), 3(c), 4(b), 4(c)), V

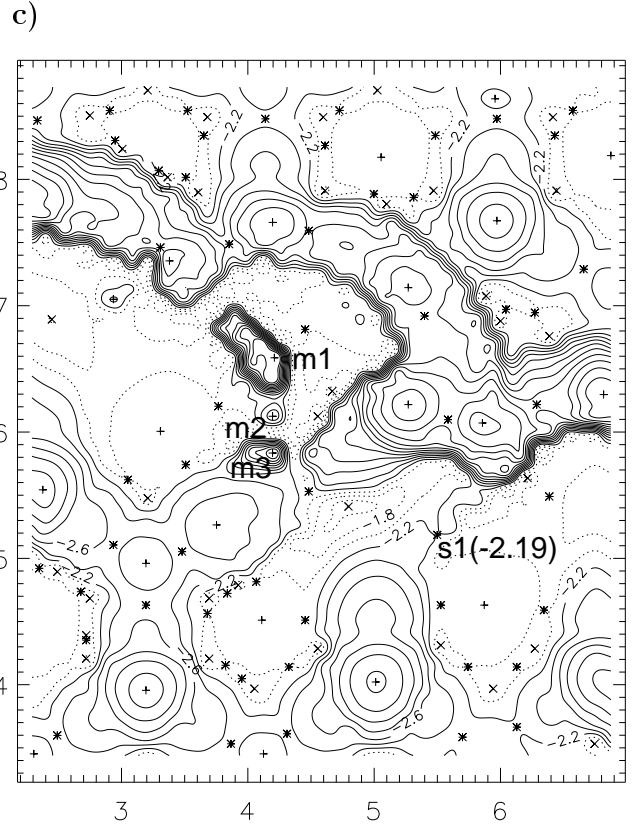
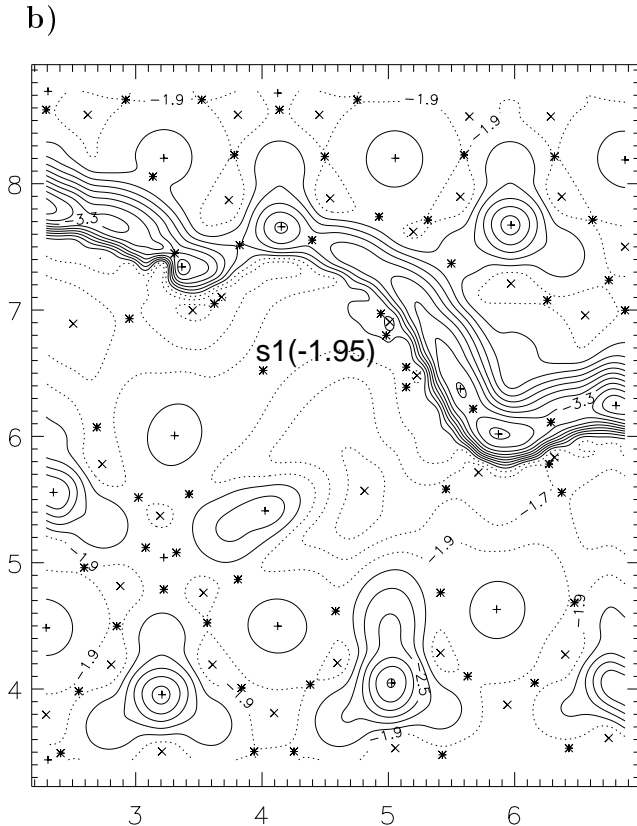
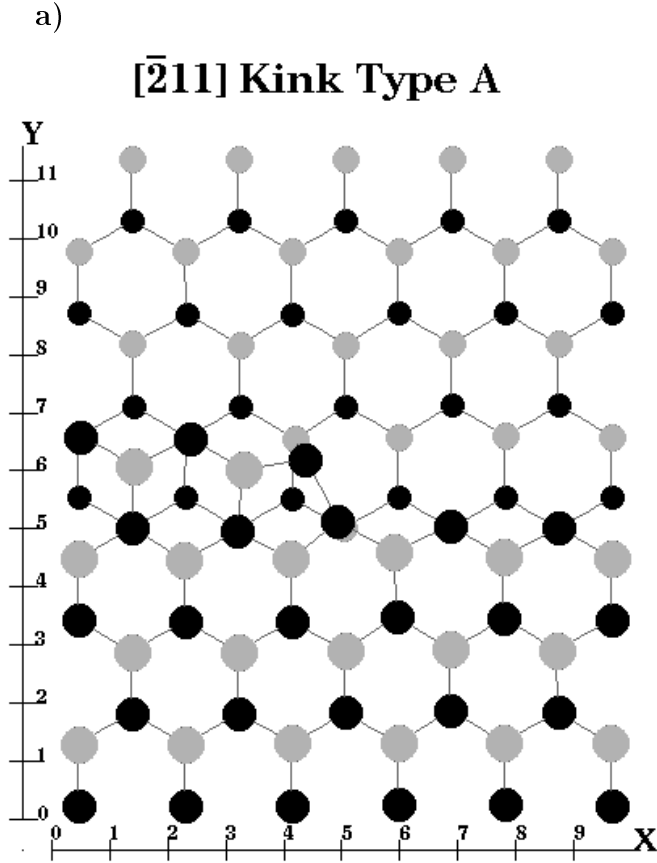


FIG. 3. Shown in (a) is the top view of the kink with re-bonding along the kink site with the upper terrace atoms larger than those on the lower terrace. (b) shows the corresponding adatom potential energy derived from the local geometry (V_{lg}) whereas (c) shows the true adatom potential energy (V). In both plots, contours are separated by 0.2 eV with the minima, saddle points and maxima marked (and sometimes labeled) by +(m),*(s) and \times (M) respectively. Figures in parenthesis are corresponding values in eV. Contours in (b) ≥ -1.9 eV and those in (c) ≥ -2.0 eV are marked with dashed lines.

and V_{lg} are computed on a rectangular grid with the spacing between points being $\frac{a_1}{16}$ ($\frac{a_2}{30}$) along the x (y) axis for a total length of $2\frac{1}{2}a_1$ ($1\frac{2}{3}a_2$). An interpolation scheme applying periodic boundary conditions along the x and y axes similar to that used in the simulations, was used to construct the contour plots of Fig. 3. From our previous study¹⁰, the error in V due to (the same) finite grid size and similar interpolation scheme was estimated to be ± 0.05 eV. We therefore assume here that this error remains the same. Being much larger than the errors due to finite size effects, it is assumed to be the error bar in V . Barrier values being differences are therefore estimated to have an error bar of ± 0.07 eV.

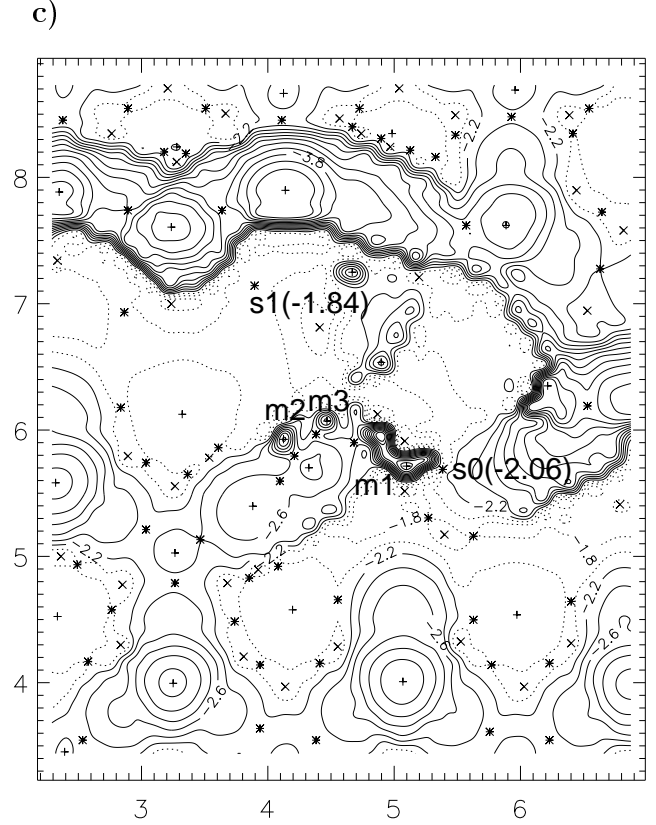
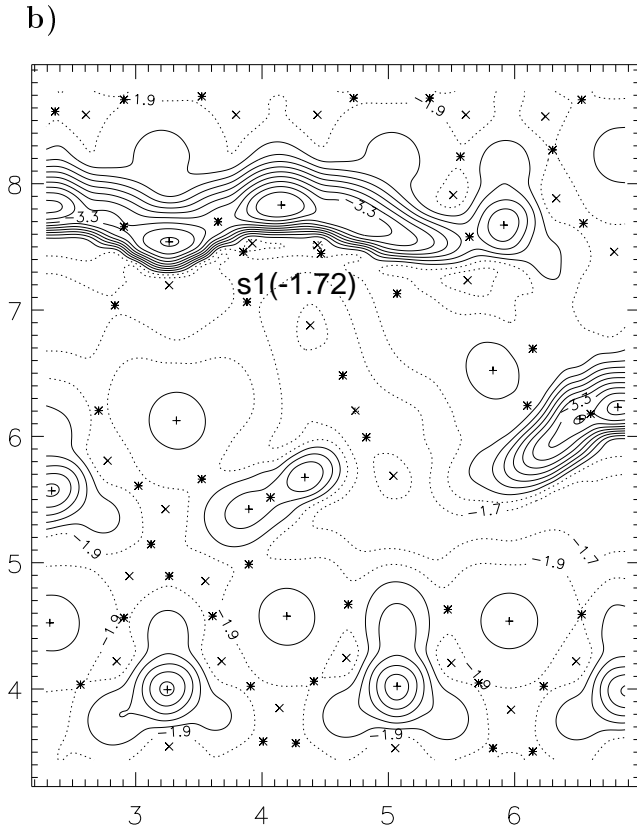
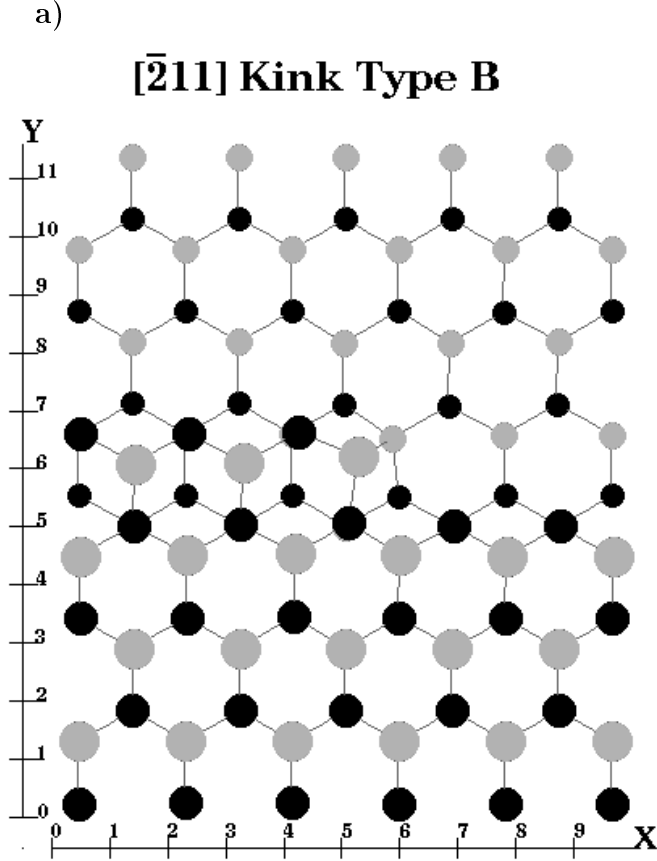


FIG. 4. Shown in (a) is the top view of the kink with an atom of the upper terrace (larger atoms) rebonded to the lower terrace. (b) shows the corresponding adatom potential energy derived from the local geometry (V_{lg}) whereas (c) shows the true adatom potential energy (V). In both plots, contours are separated by 0.2 eV with the minima, saddle points and maxima marked (and sometimes labeled) by $+$ (m), $*$ (s) and \times (M) respectively. Figures in parenthesis are corresponding values in eV. Contours in (b) ≥ -1.9 eV and those in (c) ≥ -2.0 eV are marked with dashed lines.

III. DISCUSSION

As mentioned previously, we have attempted to identify robust features of this study as those that follow from changes in adatom coordination number. Here, we assume (as before¹⁰) that the adatom potential energy obtained from relaxing only the adatom over the relaxed (but fixed) adatom free configurations (V_{lg}) to be a good measure of its coordination number. Previously we had argued¹⁰ that features that follow from a strong correlation between V_{lg} and V are robust, *i.e.*, would survive changes in details of the empirical potential used and are expected to be reproduced in more satisfactory *ab initio* or tight binding calculations. Specifically, it was assumed that if the saddle point determining the Schwoebel barrier in V_{lg} was nearly at the same position as that in V then the Schwoebel barrier is a robust feature. We now

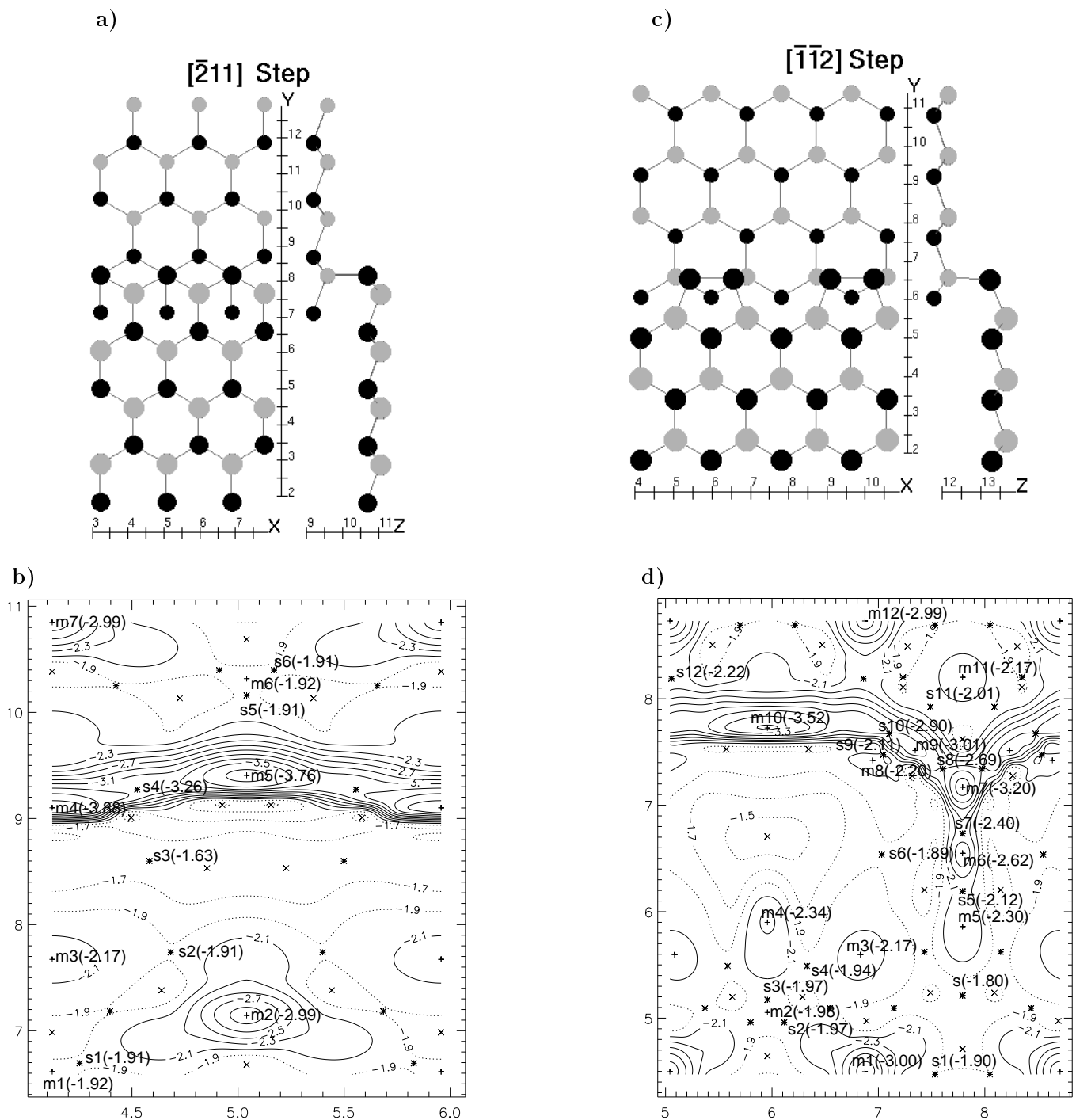


FIG. 5. In the step configurations ((a) and (d)) the upper terrace atoms are shown larger than those on the lower terrace and within each terrace the upper monolayer is in grey and the lower in black. (b) and (d) show the adatom potential energy derived from the local geometry (V_{lg}) corresponding to (a) and (c) respectively. In these plots contours are 0.2 eV apart with those ≥ -1.9 eV shown by dashed lines. The minima, saddle points and maxima are marked (labeled) by +(m), *(s) and \times (M) respectively with the figure in parenthesis being their corresponding value in eV.

argue that even if the position of the relevant saddle points differed, there is however a bound on the Schwoebel barrier that follows purely from V_{lg} - this is the difference between V_{lg} at barrier determining saddle point on the step or kink configurations and V at the

diffusion barrier determining saddle point on the free Si(111) surface. It is a strict upper bound on the Schwoebel barrier (that follows from V on the step or kink configuration) since any relaxation that occurs during the computation of V can only reduce the relevant

saddle point energy. As this bound is completely independent of the details in V , we argue that it must be a robust feature.

From the contour plots of V_{lg} corresponding to the kinks studied here (Figs. 3(b) and 4(b)) as well as the same corresponding to straight steps studied previously¹⁰ (Figs. 5(b) and 5(c)) a common trend emerges - the bound on the Schwoebel barrier (or equivalently the energy of the barrier determining saddle point in V_{lg}) is small (or more negative) when atoms at the step edge or kink site are rebonded. It can be seen (from Figs. 3 and 5) that this saddle point ($s1$ in Fig. 3(b), $s1$ in Fig. 4(b), $s3$ in Fig. 5(b) and $s6$ in Fig. 5(d)) is in the neighborhood of an upper terrace atom that has moved from its bulk terminated position in a direction away from the saddle point due to the presence of rebonding at the step edge or kink site. The magnitude of this displacement (in the $x - y$ plane) is found to be correlated to the saddle point energy which is more negative if the displacement is large. The displacement (and the relevant saddle point energy) for the $\overline{[211]}$ kinks of types A, B, the $\overline{[211]}$ step and the $\overline{[112]}$ step is 0.99\AA (-1.95 eV), 0.21\AA (-1.72 eV), 0.00\AA (-1.63 eV) and 0.72\AA (-1.89 eV) respectively. Therefore the bound on the corresponding Schwoebel barrier is 0.39 eV, 0.62 eV, 0.71 eV and 0.45 eV respectively.

The true adatom potential energy V , corresponding to the kink configurations studied here, is shown in Figs. 3(c) and 4(c). These plots show discontinuities near the kink site indicated by the presence of minima, some of which are labeled in the figures. Studying the final atomic configuration when the adatom is in these regions shows that the discontinuities are due to large scale rearrangements of atoms leading to a loss in the identity of the adatom. In other words, in these configurations, the adatom seems to occupy a lattice position after dislodging another atom which now appears to be the adatom. Diffusion in these regions cannot therefore be viewed as a *single* atom process, thereby making the contour plots in these regions less meaningful. The saddle point determining the Schwoebel barrier in case of the $\overline{[211]}$ kink of type A ($s1$ in Fig. 3(c)) is however not in the proximity of such regions. Therefore the corresponding Schwoebel barrier of 0.15 ± 0.07 eV is assumed to be relevant for processes involving only a single adatom. In the case of the kink of type B, it appears that $s0$ (in Fig. 4(c)) is the relevant saddle point that determines the Schwoebel barrier. However, this point is close to a minimum that indicates a discontinuity in V . The Schwoebel barrier determined by this point (0.28 ± 0.07 eV) is therefore considered as corresponding to a multi atom, and not a single atom, process. Hence, discounting this point, the Schwoebel barrier (determined by $s1$ in Fig. 4(c)) is 0.50 ± 0.07 eV.

In our previous study of barriers over straight steps,¹⁰ discontinuities in V , of the kind that are seen here, were not observed. This was because the temperature used during the simulation was very small - $\approx 2 \times 10^{-4}$ eV. Here we used a larger temperature ($\approx 3 \times 10^{-3}$ eV) which

resulted, in the presence of the adatom, the large scale movement of atoms around the kink site. The experimentally relevant temperature⁹ however continues to be much larger - ≈ 0.1 eV. At these temperatures we expect multi-atom processes to have smaller Schwoebel barriers - this is supported by the observation here that such a process occurs near the $\overline{[211]}$ kink of type B with the Schwoebel barrier being smaller than that for the single atom process. The general decrease in the barrier values is however consistent with the small upper bound on the Schwoebel barrier (0.05 eV) developed previously¹⁰ from an analysis of experimental data on the electromigration of steps.⁹

IV. CONCLUSION

Schwoebel barriers, calculated using the empirical Stillinger-Weber potential, for unit depth kinks along the $\overline{[211]}$ step are smaller in magnitude as compared to that calculated previously¹⁰ for the straight $\overline{[211]}$ step. This decrease can be expected directly from the adatom potential energy plots (V_{lg}) that follow purely from the local geometry of atoms around the adatom in these atomic configurations. These plots as well as similar plots for the straight $\overline{[211]}$ and $\overline{[112]}$ steps calculated previously¹⁰ show that the upper bound on the true Schwoebel barrier calculated using V_{lg} is correlated to the displacement of an atom on the upper terrace of these configurations that is near the relevant saddle point in V_{lg} . The true adatom potential energy plots (V) however show discontinuities due to large scale movement of atoms near the kink sites resulting sometimes in smaller barriers than when such movements do not occur. We therefore speculate that multi-atom processes occurring in the configurations studied here and previously¹⁰ could have smaller Schwoebel barriers.

V. ACKNOWLEDGMENTS

This work has been supported by the NSF-MRG and the U.S. ONR.

¹ R.L. Schwoebel and E.J. Shipsey, J. Appl. Phys **37**, 3682 (1966)

² M.D. Johnson, C. Orme, A.W. Hunt, D. Graff, J. Sudijono, L.M. Sander and B.G. Orr, Phys. Rev. Lett. **72**, 116 (1994)

³ M. Siegert and M. Plischke, Phys. Rev. Lett. **73**, 1517 (1994)

⁴ A.W. Hunt, C. Orme, D.R.M. Williams, B.G. Orr and L.M. Sander, Europhys. Lett. **27**, 611 (1994)

⁵ I. Elkinani and J. Villain, J. Phys. I (France) **4**, 949 (1994)

- ⁶ C.J. Lanczycki and S. Das Sarma, Phys. Rev. Lett. **76**, 780 (1996)
- ⁷ J.Villain, J. Phys. *I* **1**, 19 (1991)
- ⁸ A.V. Latyshev, A.L. Aseev, A.B. Krasilnikov and S.I. Stenin, Surf. Sci. **213**, 157 (1989)
- ⁹ E.D. Williams, E. Fu, Y.N. Yang, D. Kandel and J.D. Weeks, Surf. Sci. **336**, L746 (1995)
- ¹⁰ S. Kodiyalam, K.E. Khor and S. Das Sarma, to appear in Phys. Rev. B (1996)
- ¹¹ S. Kodiyalam, K.E. Khor, N.C. Bartelt, E.D. Williams and S. Das Sarma, Phys. Rev. B **51**, 5200 (1995)